

**FULL PAPER**

# Synthesis, characterization, and biocompatibility assessment of manganese carbonate nanoparticles stabilized with methylcellulose for multifaceted application in medicine

Andrey Blinov<sup>a</sup>  | Zafar Rekhman<sup>a</sup>  | Alexey Gvozdenko<sup>a</sup>  | Sergey Piskov<sup>a</sup>  | Vadim Agzamov<sup>b</sup>   
| Nikita Omelianov<sup>b</sup>  | Zelimhan Chagaev<sup>b</sup>  | Daria Morzaleva<sup>b</sup>  | Iuliia Ismagilova<sup>b</sup>  | Daria Gadaeva<sup>b</sup>  | Marina Poladashvili<sup>c</sup>  | Andrey Nagdalian<sup>a,\*</sup> 

<sup>a</sup>North Caucasus Federal University, Stavropol, Russia

<sup>b</sup>Bashkir State Medical University, Ufa, Russia

<sup>c</sup>Russian University of Medicine, Moscow, Russia

This work presents a study on the synthesis, characterization, and biocompatibility assessment of manganese carbonate nanoparticles (MC-NPs) stabilized with methylcellulose. Manganese acetate was used as a manganese-containing precursor, ammonium carbonate was used as a precipitator, and methylcellulose served as a stabilizing agent. The samples obtained exhibited a size distribution described as monomodal, though the relatively large standard deviation ( $\pm 80$  nm) suggests some variability, which should be noted. The average hydrodynamic radius was measured as  $393 \pm 80$  nm. The phase composition of the samples was identified as manganese carbonate ( $\text{MnCO}_3$ ) with a rhombohedral crystal lattice belonging to the R-3c spatial group. MC-NPs samples were composed of spherical aggregates with diameters ranging from 0.4 to 2  $\mu\text{m}$ . Quantum chemical modeling and IR spectroscopy revealed that the interaction between manganese carbonate and methylcellulose occurs through the OH- group attached to the C4 atom of the glucopyranose residue. While this interaction mechanism is briefly summarized, its specific relevance to the biocompatibility of the nanoparticles warrants further clarification. The biocompatibility of the obtained samples was evaluated using the chorioallantois membrane model of a chicken embryo and histological analysis. Results demonstrated that MC-NPs stabilized with methylcellulose are biocompatible, non-toxic, and hold great potential for multifaceted applications in medicine.

**\*Corresponding Author:**

Andrey Nagdalian

Email: [aanagdalian@yandex.ru](mailto:aanagdalian@yandex.ru)

Tel.: +79886783186

**KEYWORDS**

Nanomaterials; nano medicine; toxicity; CAM assay.

**Introduction**

Manganese carbonate nanoparticles (MC-NPs) have found wide application in various

branches of science and technology [1,5]. Thus, MC-NPs are used in supercapacitors [6,9]. For instance, Karuppaiah *et al.* [6] found that supercapacitors based on MC-NPs

demonstrate a high specific energy of 18.07 W/h·kg<sup>-1</sup>, a power density of 7498 W/h·kg<sup>-1</sup> and excellent capacity retention of 98.79% even after 10,000 cycles. MC-NPs are used to determine the concentration of various substances. Notably, Xu *et al.* [10] manufactured a biosensor based on MC-NPs and reached excellent performance in the electrocatalytic reduction of H<sub>2</sub>O<sub>2</sub>. The linear range of H<sub>2</sub>O<sub>2</sub> detection ranged from 0.06 to 40.0 μM with a detection limit of 0.015 μM.

It is known about the use of MC-NPs in medicine, in particular for magnetic resonance imaging (MRI) [11,13], for drugs delivery to target organs [14], for sonodynamic therapy [15], etc. Cheng *et al.* [11] demonstrated the effectiveness of using MC-NPs with polydopamine sheathing for photothermal tumor ablation under MRI control *in vivo* by intra-tumor injection in mice with 4T1 tumors. The result of the MRI shows a significantly brighter MR image in the tumor area. The authors associated the high therapeutic efficacy with the high efficiency of photothermal transformation. Given that Mn is an essential trace element and participates in the regulation of many biochemical processes, its organic forms are used in medicine and pharmacy as bioavailable sources of Mn [16,18]. Interestingly, Mn is involved in the main neurochemical processes in the central nervous system, in the formation of bone and connective tissues, regulation of fat and carbohydrate metabolism, metabolism of vitamins C, E, choline, and B vitamins [19,21].

Currently, researchers use various methods for synthesis of MC-NPs [22,26]. Wang *et al.* [22] suggested a method for the production of MC-NPs doped with Gd, which consisted in the thermal decomposition of a mixture of manganese oleate with gadolinium oleate at 310 °C. The authors found that MC-NPs doped with Gd can be obtained only if the concentration of Gd is in the range from 20 to 33 mol.%. Notably, the uniformity of the obtained MC-NPs doped with Gd improves

with increasing synthesis temperature and increasing synthesis time. Karuppaiah *et al.* [6] synthesized MC-NPs by hydrothermal and microwave methods and obtained samples with developed porous structure. In parallel, the synthesis of spherical MC-NPs under supercritical conditions was presented by Lee *et al.* [23]. The authors used manganese acetate as a precursor, which was carbonized with carbon dioxide under supercritical conditions. The obtained samples had developed porosity with the inner surface area of the pores of about 83 m<sup>2</sup>/g and the specific capacity of 322 F·g<sup>-1</sup>. Lu *et al.* [24] produced spherical MC-NPs by chemical deposition. The authors revealed that when sodium sulfate was added to the reaction mixture, the MC-NPs morphology changed from spherical to cubic shape. The obtained material has a porous structure and can be used for photocatalysis.

For the use of MC-NPs in medicine, it is necessary to justify that the nanoparticles do not have a toxic effect on a living organism. One of the ways to reduce the toxicity and increase the biocompatibility of MC-NPs is to form a shell consisting of a biocompatible material on the nanoparticles surface. For instance, Jiang *et al.* [27] synthesized MC-NPs consisting of an inner MnCO<sub>3</sub> core and an outer shell made of a platelet membrane. The presence of a platelet membrane provides PMC with excellent biocompatibility and the ability to actively target, which allows for precise destruction of cancer cells. *In vitro* experiments showed that combined treatment using PMC completely suppresses the formation of stem cells. In other work, Meng *et al.* [28] obtained a biocompatible composite material consisting of MC-NPs, Ag NPs, and polydiallyldimethylammonium chloride. Thus, the correct selection of stabilizing agent for MC-NPs is critically important for formulation of biocompatible and non-toxic material.

Thus, the aim of this work was to develop and study biocompatible MC-NPs stabilized

with methylcellulose for biomedical applications.

While the biomedical focus of this study highlights the potential of MC-NPs for MRI contrast enhancement, drug delivery, and therapy, these applications are described without fully addressing the challenges or gaps in existing methods. By comparison, the introduction of MC-NPs emphasizes their use in super-capacitors at greater length, creating an imbalance in focus. Future work should aim to better contextualize the biomedical applications of MC-NPs, particularly by identifying limitations in current techniques and presenting how MC-NPs might overcome these challenges.

## Experimental

### *Synthesis and characterization of MC-NPs stabilized with methylcellulose*

The MC-NPs synthesis stabilized with methylcellulose was performed as follows: A 0.8 M solution of manganese acetate was mixed with a 1% solution of methylcellulose in a beaker and stirred on a magnetic stirred for 10 minutes at a speed of 500 rpm. The temperature during this process was not specified and should be clarified to ensure reproducibility. Subsequently, a 0.8 M ammonium carbonate solution was added dropwise to the mixture. The resulting precipitate was centrifuged five times for 5 minutes at 3000 rpm, followed by drying at 110 °C for 8 hours. While the drying process appears sufficient for water removal, the rationale for selecting these specific conditions over alternative drying methods (e.g., vacuum drying or freeze-drying) should be provided to improve reproducibility.

MC-NPs stabilized with methylcellulose were characterized using X-ray phase analysis performed with an Empyrean 2 X-ray diffractometer (PANalytical B.Y, the Netherlands). The microstructure of the samples was analyzed using a MIRA-LMH

scanning electron microscope (SEM) equipped with the AZtecEnergy Standard/X-max 20 elemental composition determination system (Tescan, Czech Republic). Fourier-transform infrared (FTIR) spectroscopy was conducted using an FSM 1201 spectrometer (Infraspek, Russia) to investigate the structural features. The average hydrodynamic radius of the particles was determined by dynamic light scattering (DLS) on the Photocor-Complex instrument (Photokor, Russia), and data analysis was conducted using the DynaLS software. To understand the interaction between manganese carbonate and methylcellulose, quantum chemical modeling was performed using QChem software with the IQmol molecular editor (Q-Chem Inc., Pleasanton, CA, USA). The calculations employed the B3LYP method, a 6-31G\* basis set, and convergence criteria of 5. These calculations were conducted at the North Caucasus Federal University's data processing center (Schneider Electric, Ratingen, Germany).

### *CAM assay*

The MC-NPs biocompatibility was evaluated *in vivo* using the chorioallantoic membrane (CAM) model of a chicken embryo. The procedure followed the methodologies outlined by Coelho et al. [29], Shendage et al. [30], and Rzhepakovsky et al. [31], with slight modifications.

Fertilized chicken eggs of the Haysex Brown cross were sourced from Agrokormservice Plus (Adygea, Russia). The eggs were disinfected with 70% ethanol and incubated in an Rcom Maru Deluxe Max 380 digital incubator (AUTOELEX CO., Korea) at 37.6 °C and 55% humidity, with automatic tray rotation every hour. On the 3<sup>rd</sup> day of incubation, 3 mL of albumen was aspirated from the blunt end of the egg under sterile conditions using a syringe, and the opening was sealed with paraffin wax. A window measuring 2.5 cm<sup>2</sup> was then created on the

eggshell and covered with transparent tape. The eggs were returned to the incubator for further development.

On the 8<sup>th</sup> day of incubation, MC-NPs powder samples were UV-sterilized using an ultraviolet irradiator ("Azov" OBN-35-01 UHL 4.2, St. Petersburg, Russia). A 10 mg powder sample was placed on the CAM surface using a sterile silicone ring (inner diameter 5 mm, thickness 1.5 mm) to mark the application area. However, the rationale for choosing 10 mg as the test quantity was not discussed and should be clarified, particularly in the context of its clinical relevance. The CAM with an empty silicone ring served as a negative control. After applying the samples, the shell windows were resealed, and incubation continued until day 14.

On day 14, CAM tissues were photographed in ovo before the embryos were euthanized in a gas chamber with 70% CO<sub>2</sub> for 30 minutes, following humane euthanasia guidelines [32]. CAM sections in contact with MC-NPs were excised and visualized ex ovo under an ARSTEK SZ0850 stereomicroscope (Beijing, China). Images were captured with a 38 MP Samega V6 digital camera and analyzed using S-EYE2.0 software (YOUNG WIN Technology Co., Beijing, China).

#### *Histological examination*

CAM tissues in contact with the MC-NPs samples were fixed in 10% buffered formalin

for 72 hours, dehydrated in isopropyl alcohol, and embedded in Histomix medical paraffin (Biovitrum, Saint Petersburg, Russia). Sections 6 μm thick were prepared using a Thermo Fisher Scientific NM 325 rotary microtome (Waltham, USA). Histological staining was conducted with hematoxylin and eosin. However, no mention was made of controls to validate staining quality, nor were measures to minimize embedding artifacts described, which should be addressed in future studies.

Histological slides were examined under an Axio Imager 2 microscope (Carl Zeiss Microscopy, Oberkochen, Germany) equipped with the AxioCam MRc5 imaging system. Images were analyzed using Zen 2 Pro software (Carl Zeiss Microscopy, Oberkochen, Germany).

#### **Results and discussion**

Initially, the average hydrodynamic radius of MC-NPs stabilized with methylcellulose was studied. The resulting histogram of the particle size distribution, depicted in Figure 1, shows a unimodal distribution with the majority of particles concentrated around a single size range. The polydispersity index (PDI) was calculated to assess the degree of size uniformity. A low PDI indicates a narrow size distribution, while a higher PDI suggests greater variability in particle size. This analysis confirms the relatively consistent size of the MC-NPs.

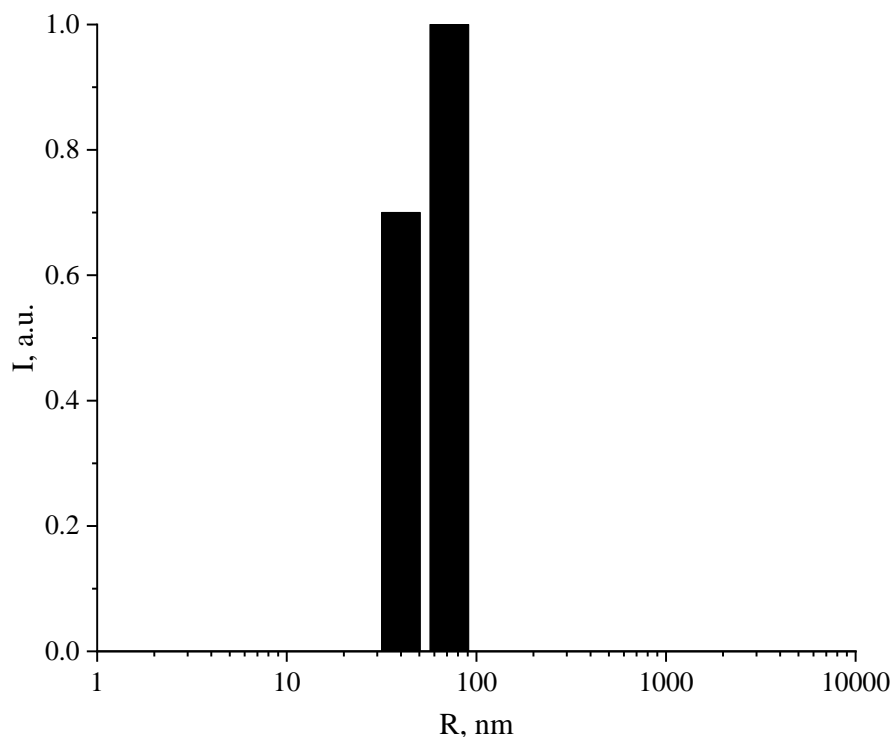


**FIGURE 1** Histogram of the distribution of the hydrodynamic radius of MC-NPs stabilized with methylcellulose

Analysis of the resulting histogram showed that the sample has a monomodal size distribution. The average hydrodynamic radius was  $393 \pm 80$  nm. Further, the resulting

sample was examined by X-ray phase analysis. The resulting diffractogram is depicted in Figure 2.

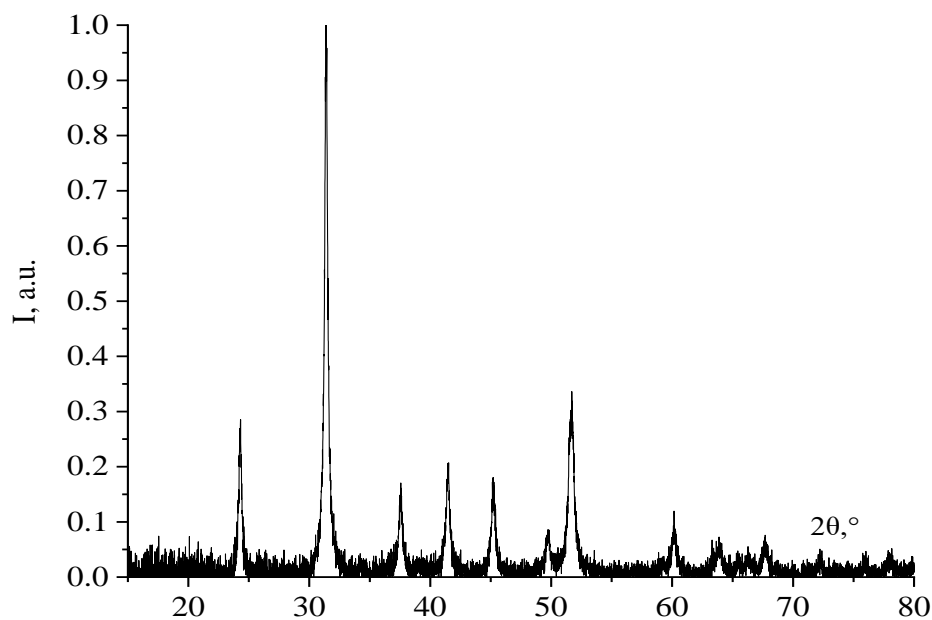


**FIGURE 2** Diffractogram of MC-NPs stabilized with methylcellulose

Analysis of the resulting diffractogram showed that the sample consists of manganese carbonate ( $\text{MnCO}_3$ ) with a rhombohedral crystal lattice of the space

group R3c. At the next stage, the obtained sample was examined by SEM. The resulting SEM micrographs are presented in Figure 3.

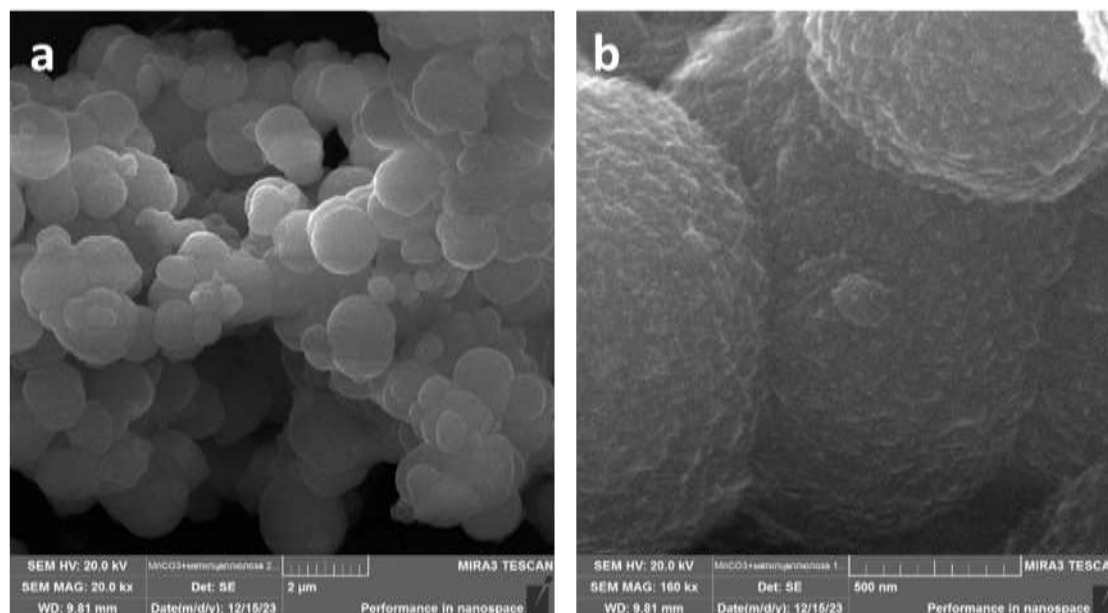


**FIGURE 3** SEM-micrographs of MC-NPs stabilized with methylcellulose at magnifications  $\times 20,000$  (a) and  $160,000$  (b)

The analysis of Figure 3 showed that the sample includes spherical aggregates with a diameter of  $0.4\text{--}2\ \mu\text{m}$ . Aggregates are formed from MC-NPs of  $50\text{--}170\ \text{nm}$ . It is important to note that the particles had a developed surface.

As a result of quantum chemical modeling of the interaction of MC-NPs with methylcellulose, molecular models and quantum chemical calculations were obtained and presented in Table 1 and Figure 4.

**TABLE 1** Results of quantum chemical modeling of the interaction of MC-NPs with methylcellulose

Type of interaction	$E$ , kkal/mol	$\Delta E$ , kkal/mol	$E_{\text{HOMO}}$ , eV	$E_{\text{LUMO}}$ , eV	$\eta$ , eV
A section of the methylcellulose molecule	-1455.031	-	-0.229	0.041	0.135
Through hydroxyl group attached to C3 atom of the glucopyranose residue	-2868.107	1413.076	-0.095	-0.016	0.040
Through hydroxyl group attached to C4 atom of the glucopyranose residue	-2868.161	1413.130	-0.098	0.000	0.049

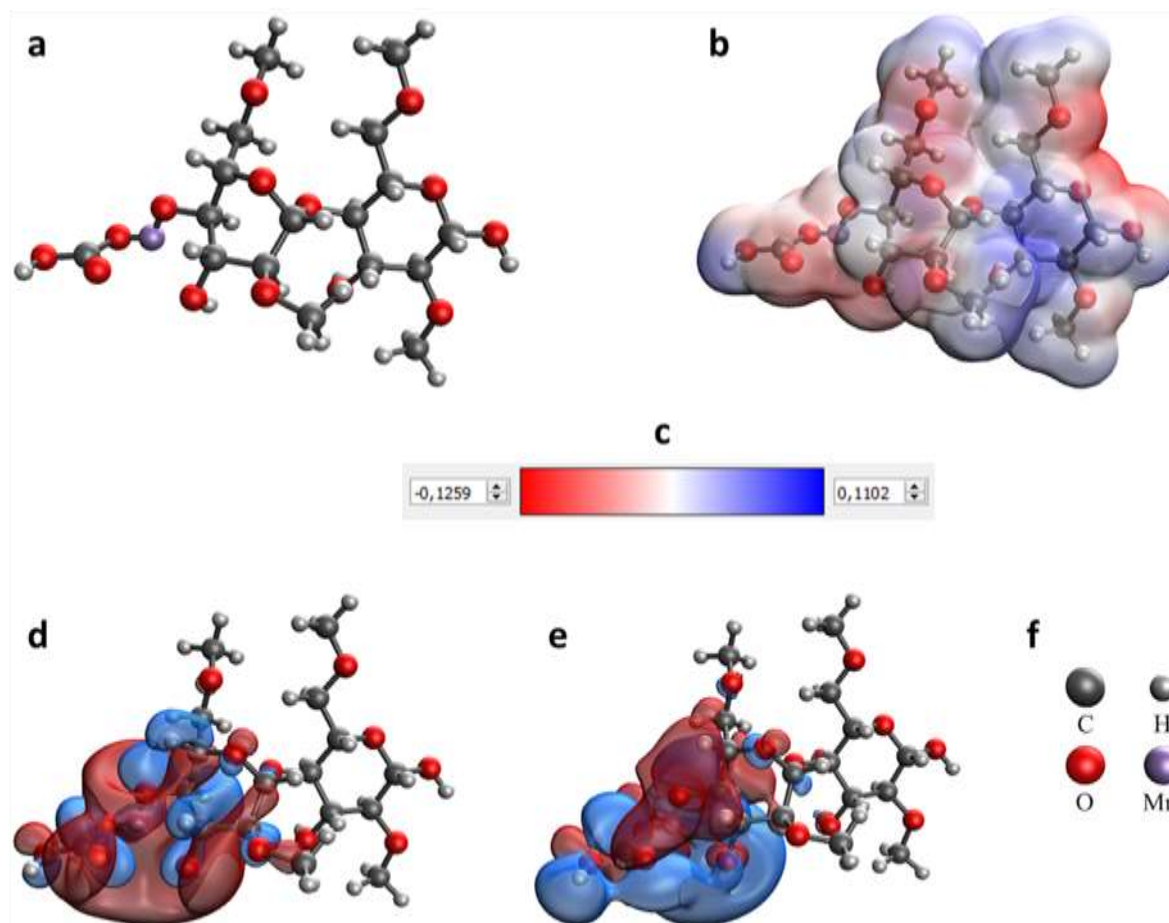


**FIGURE 4** The results of quantum chemical modeling of the interaction of MC-NPs and methylcellulose through hydroxyl group attached to C4 atom of glucopyranose residue of methylcellulose: model of molecular complex (a), distribution of electron density (b), the gradient of the distribution of electron density (c), the highest occupied molecular orbital HOMO (d), the lowest unoccupied molecular orbital LUMO (e), and decoding of atoms (f)

Based on the analysis of the data obtained, it was found that all the presented compounds are energetically advantageous ( $\Delta E > 1413.070$  kcal/mol). Based on the optimal values of chemical hardness and the difference in total energy, the most likely variant of the interaction of MC-NPs with methylcellulose was determined. Thus, the optimal interaction ( $\Delta E = 1413.130$  kcal/mol;  $\eta = 0.049$  eV) occurs through hydroxyl group

attached to C4 atom of glucopyranose residue of methylcellulose. It can be concluded that the chemical interaction between MC-NPs and methylcellulose is formed, which is due to a shift in electron density and the formation of molecular orbitals in the zone of interaction between molecules.

At the next stage, the obtained samples were examined by IR spectroscopy. The results are shown in Figure 5.

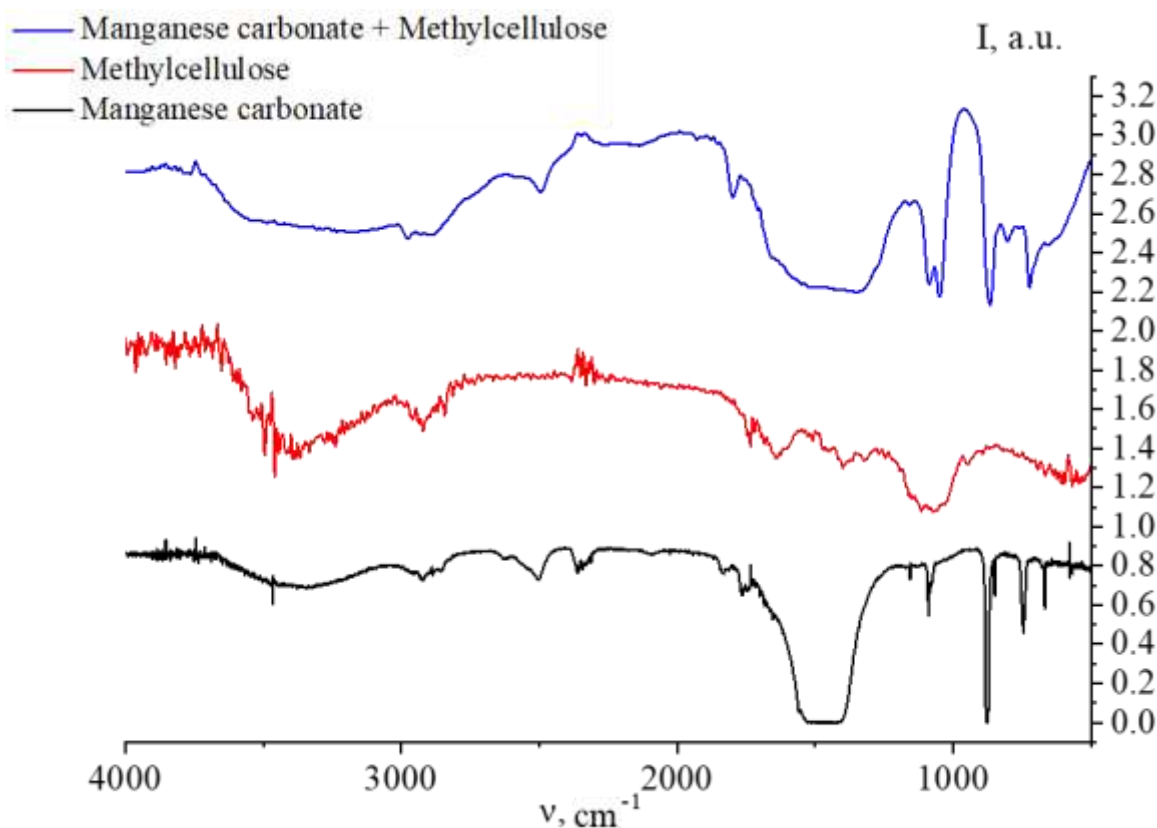


**FIGURE 5** IR-spectra of MC-NPs stabilized with methylcellulose

An analysis of the IR spectrum of MC-NPs showed that the sample contains oscillation bands characteristic of manganese carbonate: Mn-O oscillation band ( $576\text{ cm}^{-1}$ ), the C-O and C=O valence band in the  $\text{CO}_3^{2-}$ -group ( $725\text{ cm}^{-1}$ ), the C-O out-of-plane oscillation band and C=O in the  $\text{CO}_3^{2-}$  group ( $862\text{ cm}^{-1}$ ), the band of C-O and C=O asymmetric and symmetric vibrations in the  $\text{CO}_3^{2-}$  group ( $1451\text{ cm}^{-1}$ ), C=O valence bond vibrations ( $1796\text{ cm}^{-1}$ ) [33-36]. The Mn-OH bond oscillations are also present in the sample, which correspond to bands at  $1075$  and  $1155\text{ cm}^{-1}$ , as well as the C-O oscillation band ( $1055\text{ cm}^{-1}$ ) [37,38].

Analysis of the IR spectrum of methylcellulose showed that in the region from  $2800$  to  $3500\text{ cm}^{-1}$ , the presence of bands of valence bond oscillations is observed: at the  $2841\text{ cm}^{-1}$  site there are symmetrical vibrations of the  $-\text{CH}_2$  and  $-\text{CH}$  groups, at  $3478\text{ cm}^{-1}$  there are longitudinal symmetrical vibrations of the OH- group of methylcellulose

[39,40]. In the IR spectrum of methylcellulose in the range from  $1000$  to  $1700\text{ cm}^{-1}$ , bands characteristic of valence vibrations are observed: a band at  $1082\text{ cm}^{-1}$  corresponds to symmetrical vibrations of the C-O bond in the C-O-H group, a band at  $1478\text{ cm}^{-1}$  corresponds to vibrations of the  $\text{CH}_3$  bond, a band at  $1622\text{ cm}^{-1}$  oscillations of the C-H bond, a band at  $1680\text{ cm}^{-1}$  – symmetric oscillations of the C-O group [41]. In the area from  $500$  to  $950\text{ cm}^{-1}$ , bands characteristic of deformation vibrations are observed in the IR spectrum of methylcellulose: the area from  $661$  to  $685\text{ cm}^{-1}$  corresponds to out-of-plane vibrations of the OH- group, the section at  $885\text{ cm}^{-1}$  corresponds to the  $-\text{CH}_3$  bond, the section at  $939\text{ cm}^{-1}$  corresponds to vibrations of the methoxy group  $-\text{O}-\text{CH}_3$  [42]. At  $520$  and  $561\text{ cm}^{-1}$ , characteristic bands are observed due to fluctuations in the  $-\text{CH}_3$  and  $-\text{CH}_2$  bonds.

Analysis of manganese carbonate nanoparticles stabilized with methyl cellulose

showed that the samples contain oscillation bands characteristic of manganese carbonate: a low-intensity Mn–O oscillation band ( $580\text{--}600\text{ cm}^{-1}$ ), a low-intensity C–O and C=O valence band in the  $\text{CO}_3^{2-}$  ( $721\text{--}725\text{ cm}^{-1}$ ) group, the band of out-of-plane vibrations C–O and C=O in the  $\text{CO}_3^{2-}$  group ( $863\text{--}864\text{ cm}^{-1}$ ), the band of Mn–OH coupling vibrations ( $1073\text{--}1088\text{ cm}^{-1}$ ), the band of asymmetric and symmetrical vibrations C–O and C=O in the  $\text{CO}_3^{2-}$  group ( $1420\text{--}1480\text{ cm}^{-1}$ ), valence vibrations of the C=O bond ( $1796\text{--}1803\text{ cm}^{-1}$ ). It is important to note that in the samples there is a decrease in the intensity of bands in the range from  $580$  to  $600\text{ cm}^{-1}$ , characteristic of Mn–O bond fluctuations, compared with pure manganese carbonate.

There is also a decrease in the intensity of symmetric oscillations of the C–O bond in the C–O–H group by  $1082\text{ cm}^{-1}$ , characteristic of the IR spectrum of methylcellulose. Thus, it can be concluded that the interaction of manganese carbonate nanoparticles with methylcellulose occurs through a hydroxyl

group. The results are consistent with the data of quantum chemical modeling.

At the next stage, the bioavailability of MC-NPs stabilized with methylcellulose was studied. The CAM system of the chicken embryo acts as a full-featured *in vivo* platform for studying the reaction of tissues to various materials [43,44]. Taking into account the proven similarity of CAM tissue reactions with mammalian models, the primary biocompatibility and vascular effects of the provided powders were studied by applying samples to the CAM surface.

Implantation of MC-NPs stabilized with methylcellulose onto the CAM did not critically affect the survival of embryos up to 14 days of development. The percentage of embryo mortality in the experimental group and in the control group was 25% and 10%, respectively, which is not out of the reference range for the conditions of such experiments. The CAM reaction 6 days after implantation of the tested powder samples is demonstrated in Figure 6.

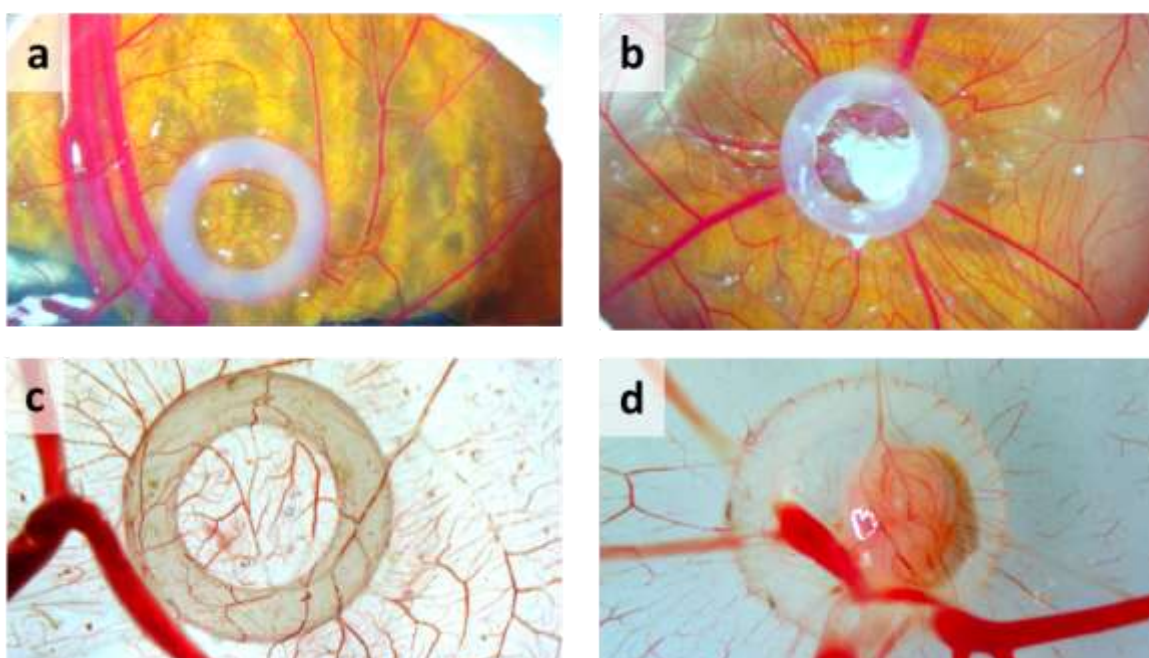


**FIGURE 6** Representative macroscopic photographs of CAM *in ovo* and the reverse side of CAM *ex ovo* 6 days after implantation of powders: a) control, b) MC-NPs stabilized with methylcellulose, c) control (reverse side of CAM *ex ovo*), and d) manganese carbonate (reverse side of CAM *ex ovo*)

The structural and surface properties of the sample of MC-NPs stabilized with methylcellulose allowed them to be absorbed on the surface of the sample while preserving the implantation site throughout the experiment. It is important to note that after 6 days of incubation, a part of the implanted powders was preserved on the surface of the CAM. A macroscopic assessment of the vascular system of the CAM in ovo after 6 days of implantation of MC-NPs stabilized with methylcellulose showed no pronounced neovascularization or decrease in vascular growth and lysis compared with the control.

For a sample of MC-NPs stabilized with methylcellulose, compared with the control in the implantation zone (center of the ring), there is an increase in vascularization in the areas of the CAM adjacent directly to the materials due to the formed new capillaries and collaterals growing towards the implantable powders. Such a vascular pattern is typical for loose and porous biocompatible materials implanted on CAM, which was noted in similar works by other researchers [45].

The results of the histological evaluation of the MC-NPs biocompatibility stabilized with methylcellulose on CAM tissues are illustrated in Figures 7 and 8.

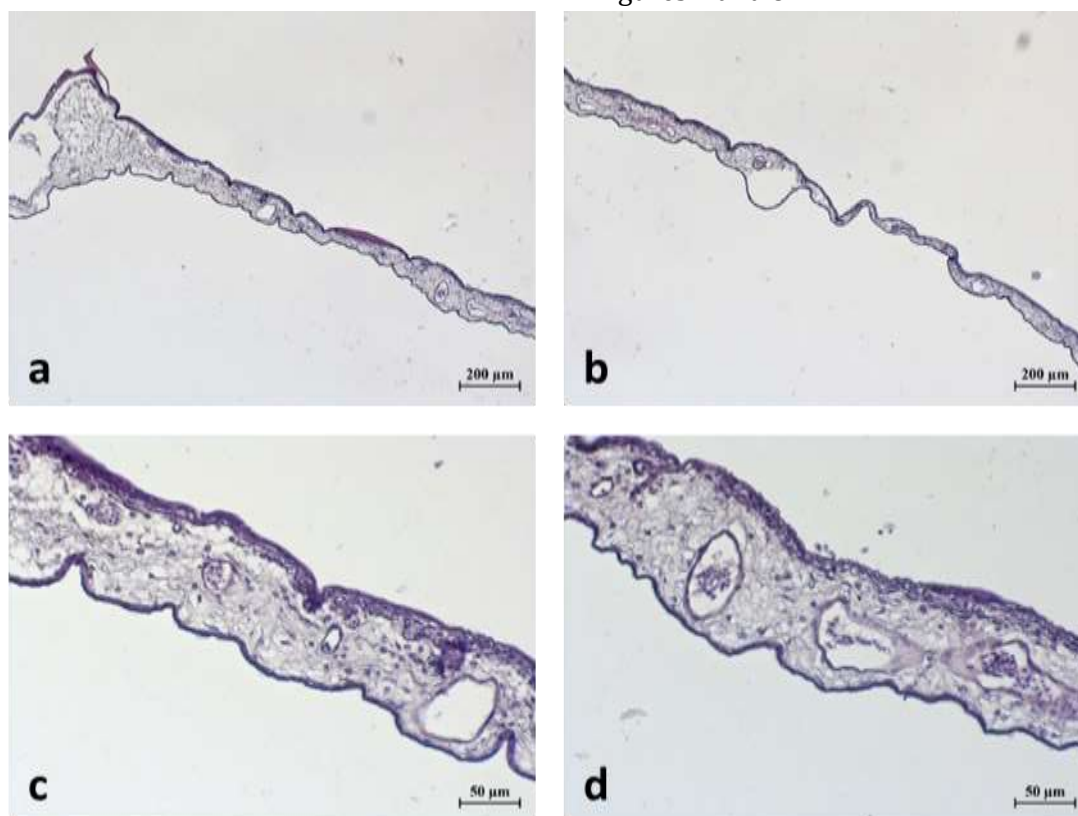


**FIGURE 7** Histological sections of the CAM with a silicone ring (control). Hematoxylin and eosin staining: a) marginal zone  $\times 50$ , b) central zone  $\times 50$ , c) marginal zone  $\times 200$ , and d) central zone  $\times 200$

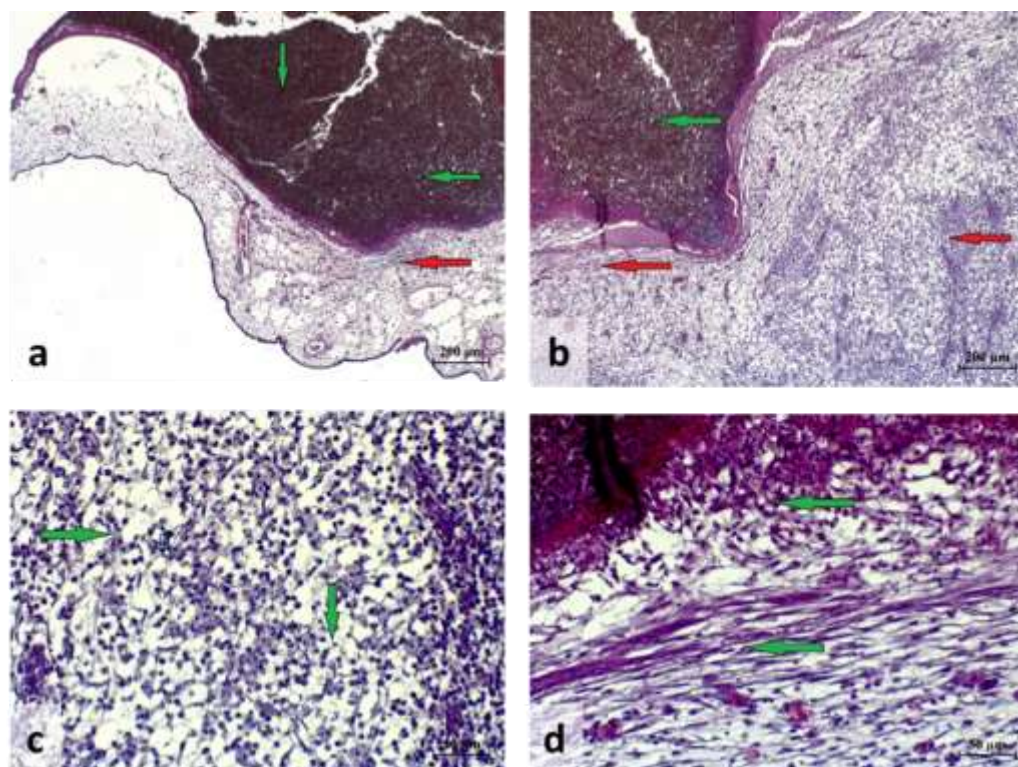


**FIGURE 8** Histological sections of the CAM with a silicone ring filled out by MC-NPs stabilized with methylcellulose: a) marginal zone  $\times 50$ , b) central zone  $\times 50$ , c) marginal zone  $\times 200$ , and d) central zone  $\times 200$

Microscopic visualization of histological sections of control sample corresponded to the characteristics of normal CAM histology described by other researchers [46,47]. It consists of an ectoderm (in contact with air/egg shells), a stroma (loose connective tissue), and an endoderm (in contact with allantois) and has a thickness of up to 200  $\mu\text{m}$ . Interestingly, MC-NPs stabilized with methylcellulose showed a pronounced tissue reaction both in the CAM stroma and in the structures of the material. This may be due not so much to their chemical properties as to weight and density. Observations made at this stage of the study using the CAM model of a chicken embryo showed that MC-NPs stabilized with methylcellulose are compatible with the biological environment of CAM.

## Conclusion

In this work, the synthesis and characterization of biocompatible MC-NPs

stabilized with methylcellulose for potential medical applications were carried out. The study of the average hydrodynamic radius of MC-NPs demonstrated a monomodal size distribution, with a mean hydrodynamic radius of  $393 \pm 80$  nm. The phase composition, as confirmed by X-ray diffraction, showed that the samples consisted of manganese carbonate ( $\text{MnCO}_3$ ) with a rhombohedral crystal lattice belonging to the spatial group R-3c. SEM micrographs revealed spherical aggregates ranging in diameter from 0.4 to 2  $\mu\text{m}$ .

Quantum chemical modeling, supported by IR spectroscopy, indicated that the interaction between MC-NPs and methylcellulose occurs primarily through the hydroxyl group attached to the C4 atom of the glucopyranose residue of methylcellulose. The calculated binding energy difference ( $\Delta E = 1413.130$  kcal/mol) and optimal chemical hardness ( $\eta = 0.049$  eV)

0.049 eV ( $\eta=0.049\text{eV}$ ) suggest a stable chemical interaction that contributes to the stabilization of MC-NPs by methylcellulose. However, further validation of these computational results through direct experimental techniques, such as detailed spectral shifts or binding energy measurements, is necessary to conclusively support these findings.

In vivo studies using the CAM model of a chicken embryo demonstrated the biocompatibility of MC-NPs stabilized with methylcellulose. No significant toxicity or adverse effects were observed on the chorioallantoic membrane, indicating compatibility with biological environments. This biocompatibility highlights the potential of MC-NPs for biomedical applications.

The study concludes that MC-NPs stabilized with methylcellulose are biocompatible and non-toxic, confirming their potential use in various biomedical applications. However, the general statement that "the chemical interaction is formed" should be supported by more quantitative data, such as experimental measurements of interaction forces or additional binding energy validations. Future research should focus on developing and characterizing advanced biomedical scaffolds based on these stabilized MC-NPs for tissue engineering applications. Further studies exploring the long-term stability, functional performance, and detailed mechanisms of interaction in biological systems would provide stronger evidence for their use in medical devices or therapies.

### Data availability

All raw data are available upon request from the corresponding author.

### Acknowledgments

The authors express their gratitude to Dr. Igor Rzhepakovsky for valuable assistance in in vivo experiments.

### Funding

The work was financially supported by the Ministry of Science and Higher Education of the Russian Federation (project FSRN-2023-0037).

### Authors' Contributions

Andrey Blinov: Conceptualization, Methodology, Writing-original draft, Writing-review and editing, Supervision, Funding acquisition; Zafar Rekhman: Methodology, Investigation, Writing-original draft; Alexey Gvozdenko: Methodology, Investigation, Writing-original draft; Sergey Piskov: Methodology, Investigation, Visualization, Writing-original draft; Vadim Agzamov: Formal analysis, Writing original draft, Validation; Nikita Omelianov: Resources, Writing original draft; Zelimhan Chagaev: Software; Writing original draft; Daria Morzaleva: Visualization, Writing original draft; Iuliia Ismagilova: Validation, Writing original draft; Daria Gadaeva: Investigation, Writing original draft; Marina Poladashvili: Investigation, Writing original draft; Andrey Nagdalian: Writing-review and editing, Resources, Project administration.

### Conflict of Interest

The authors declare that they have no known competing financial interests or personal relationships that could have appeared to influence the work reported in this article.

### Orcid:

Andrey Blinov:

<https://orcid.org/0000-0002-4701-8633>

Zafar Rekhman:

<https://orcid.org/0000-0003-2809-4945>

Alexey Gvozdenko:

<https://orcid.org/0000-0001-7763-5520>

Sergey Piskov:

<https://orcid.org/0000-0002-5558-5486>

Vadim Agzamov:

<https://orcid.org/0000-0001-9845-2280>

Nikita Omelianov:

<https://orcid.org/0009-0005-5397-628X>

Zelimhan Chagaev:

<https://orcid.org/0000-0002-9413-9550>

Daria Morzaleva:

<https://orcid.org/0009-0003-5283-084X>

Iuliia Ismagilova:

<https://orcid.org/0009-0004-0603-7864>

Daria Gadaeva:

<https://orcid.org/0000-0003-0670-6605>

Marina Poladashvili:

<https://orcid.org/0009-0003-8817-0003>

Andrey Nagdalian\*:

<https://orcid.org/0000-0002-6782-2821>

## References

- [1] Y. Wu, A. Wang, H. Zhao, Q. Zhang, D. Lei, C. Han, Oxygen-dependent catalytic activity of mesoporous MnCO<sub>3</sub>-based catalysts for highly effective benzene oxidation, *Fuel*, **2024**, 363, 130886. [Crossref], [Google Scholar], [Publisher]
- [2] V.P. Veeraraghavan, H.L.A. Khan, P. Veerakumar, Microwave-assisted hydrothermal synthesis of Ru-doped Mn<sub>3</sub>O<sub>4</sub> nanoflowers for biomedical applications. [Crossref], [Google Scholar], [Publisher]
- [3] J.C. Garcia, P. Barai, J. Chen, A. Gutierrez, J. Wen, I. Arslan, X. Wang, T.T. Fister, H. Iddir, V. Srinivasan, Predicting morphological evolution during coprecipitation of MnCO<sub>3</sub> battery cathode precursors using multiscale simulations aided by targeted synthesis, *Chemistry of Materials*, **2020**, 32, 9126-9139. [Crossref], [Google Scholar], [Publisher]
- [4] L. Chen, P. Zhao, L. Song, K. Luo, N. Xie, H. Wang, L. LYe, Manganese carbonate superparticles as DNA-and pH-responsive magnetic resonance imaging contrast agents, *Materials Today Nano*, **2024**, 27, 100496. [Crossref], [Google Scholar], [Publisher]
- [5] a) Z. Bahadorloo, Z. Piravar, J. Sabaghzadeh, The effect of low-level laser therapy on differentiation ability of human

- adipocyte- derived stem cells to keratinocytes, *International Journal of Advanced Biological and Biomedical Research*, **2023**, 11, 82-93. [Crossref], [Google Scholar], [Publisher]; b) B. Li, L. Han, H. Wang, Y. Zheng, Albumin-templated manganese carbonate nanoparticles for precise magnetic resonance imaging of acute myocardial infarction, *Journal of Biomaterials Applications*, **2022**, 37, 493-501. [Crossref], [Google Scholar], [Publisher]
- [6] a) E.P. Ime, E.J. Ajor, F.D.M. Ekpan, H.S. Samuel, O.P. Egwuatu, Reinforced recycled plastic composites, *Eurasian Journal of Science and Technology*, **2024**, 4, 165-178. [Crossref], [Pdf], [Publisher]; b) M. Karuppaiah, R. Akilan, P. Sakthivel, S. Asaithambi, R. Shankar, R. Yuvakkumar, Y. Hayakawa, G. Ravi, Synthesis of self-assembled micro/nano structured manganese carbonate for high performance, long lifespan asymmetric supercapacitors and investigation of atomic-level intercalation properties of OH<sup>-</sup> ions via first principle calculation, *Journal of Energy Storage*, **2020**, 27, 101138. [Crossref], [Google Scholar], [Publisher]
  - [7] D. Zhang, Y. Zhang, G. Lu, Y. Hu, X. Qiu, W. Ma, K. Zheng, Basic magnesium carbonate template assisted co-carbonization of potassium citrate toward hierarchical porous carbon for supercapacitors, *Journal of Alloys and Compounds*, **2024**, 1002, 175470. [Crossref], [Google Scholar], [Publisher]
  - [8] X. Cao, Y. Liu, Y. Zhong, L. Cui, A. Zhang, J.M. Razal, W. Yang, J. Liu, Flexible coaxial fiber-shaped asymmetric supercapacitors based on manganese, nickel co-substituted cobalt carbonate hydroxides, *Journal of Materials Chemistry A*, **2020**, 8, 1837-1848. [Crossref], [Google Scholar], [Publisher]
  - [9] V.V. Palem, Ultrasonic-assisted, rapid preparation of mesoporous MnCO<sub>3</sub> for electrochemical supercapacitor applications: A novel approach, *Journal of Electroanalytical*

- Chemistry*, **2023**, *942*, 117571. [[Crossref](#)], [[Google Scholar](#)], [[Publisher](#)]
- [10] L. Xu, J. Li, W. Shi, N. Bao, C. Yu, Immobilization of hemoglobin on MnCO<sub>3</sub> sphere-loaded Au nanoparticles as highly efficient sensing platform towards hydrogen peroxide, *Nanotechnology*, **2020**, *32*, 025503. [[Crossref](#)], [[Google Scholar](#)], [[Publisher](#)]
- [11] Y. Cheng, S. Zhang, N. Kang, J. Huang, X. Lv, K. Wen, S. Ye, Z. Chen, X. Zhou, L. Ren, Polydopamine-coated manganese carbonate nanoparticles for amplified magnetic resonance imaging-guided photothermal therapy, *ACS Applied Materials & Interfaces*, **2017**, *9*, 19296-19306. [[Crossref](#)], [[Google Scholar](#)], [[Publisher](#)]
- [12] X. Zhu, H. Xiong, Q. Zhou, Z. Zhao, Y. Zhang, Y. Li, S. Wang, S. Shi, pH-activatable MnCO<sub>3</sub> nanoparticle for improved magnetic resonance imaging of tumor malignancy and metastasis, *ACS Applied Materials & Interfaces*, **2021**, *13*, 18462-18471. [[Crossref](#)], [[Google Scholar](#)], [[Publisher](#)]
- [13] a) W. Abdussalam-Mohammed, A.Q. Ali, M. Khelifa, O. Otman, A.A. Elhadi, Highly stable gold nanoparticle functionalized by aspirin in an aqueous solution: Evaluation of its stability at different temperatures and pH values, *Chemical Methodologies*, **2024**, *8*, 521-537. [[Crossref](#)], [[Google Scholar](#)], [[Publisher](#)]; b) W. Li, Y. Wang, D. Xue, L. Jin, Y. Liu, Z. Lv, Y. Cao, R. Niu, H. Zhang, S. Zhang, B. Xu, A novel biodegradable nanoplatform for tumor microenvironments responsive bimodal magnetic resonance imaging and sonodynamic/ion interference cascade therapy, *ACS Applied Materials & Interfaces*, **2022**, *14*, 50616-50625. [[Crossref](#)], [[Google Scholar](#)], [[Publisher](#)]
- [14] K.K. Lee, J.H. Lee, S.C. Lee, C.S. Lee, MnCO<sub>3</sub>- mineralized polydopamine nanoparticles as an activatable theranostic agent for dual-modality imaging-guided photothermal therapy of cancers, *Theranostics*, **2022**, *12*, 6762. [[Crossref](#)], [[Google Scholar](#)], [[Publisher](#)]
- [15] H. Zhang, X. Pan, Q. Wu, J. Guo, C. Wang, H. Liu, Manganese carbonate nanoparticles-mediated mitochondrial dysfunction for enhanced sonodynamic therapy, In *Exploration*, **2021**, *1*, 20210010. [[Crossref](#)], [[Google Scholar](#)], [[Publisher](#)]
- [16] a) M. Khanahmadi, F. Shahrezaei, M. Sharifi, B.G. Rezanejade, Ultrasound- assisted preparation and optimization of natural flavoring nanoemulsion for dairy products based on pistacia khinjuk in lab scale, *Chemical Methodologies*, **2023**, *7*, 524-539. [[Crossref](#)], [[Google Scholar](#)], [[Publisher](#)]; b) R. Maciejewski, E. Radzikowska-Büchner, W. Flieger, K. Kulczycka, J. Baj, A. Forma, J. Flieger, An overview of essential microelements and common metallic nanoparticles and their effects on male fertility, *International Journal of Environmental Research and Public Health*, **2022**, *19*, 11066. [[Crossref](#)], [[Google Scholar](#)], [[Publisher](#)]
- [17] T. Fotina, R. Petrov, O. Shkromada, O. Nechyporenko, O. Fotin, Quality of broiler chicken meat with the addition of chelated compounds of microelements to the diet, *Ukrainian Journal of Veterinary Sciences*, **2022**, *13*. [[Crossref](#)], [[Google Scholar](#)], [[Publisher](#)]
- [18] A.C. Martins, B.N. Krum, L. Queirós, A.A. Tinkov, A.V. Skalny, A.B. Bowman, M. Aschner, Manganese in the diet: bioaccessibility, adequate intake, and neurotoxicological effects, *Journal of Agricultural and Food Chemistry*, **2022**, *68*, 12893-12903. [[Crossref](#)], [[Google Scholar](#)], [[Publisher](#)]
- [19] a) M.S. Jabar, A.L. Wadood, Cytotoxicity and anticancer effect of chitosan-Ag NPs-doxorubicin-folic acid conjugate on lungs cell line, *Chemical Methodologies*, **2023**, *7*, 1-14. [[Crossref](#)], [[Google Scholar](#)], [[Publisher](#)]; b) A. Frydrych, M. Krośniak, K. Jurowski, The role of chosen essential elements (Zn, Cu, Se, Fe, Mn)

- in food for special medical purposes (FSMPs) dedicated to oncology patients-critical review: State-of-the-art, *Nutrients*, **2023**, *15*, 1012. [[Crossref](#)], [[Google Scholar](#)], [[Publisher](#)]
- [20] M. Rondanelli, M.A. Faliva, G. Peroni, V. Infantino, C. Gasparri, G. Iannello, S. Perna, A. Riva, G. Petrangolini, A. Tartara, Essentiality of manganese for bone health: An overview and update, *Natural Product Communications*, **2021**, *16*, 1934578X211016649. [[Crossref](#)], [[Google Scholar](#)], [[Publisher](#)]
- [21] J.M. Studer, W.P. Schweer, N.K. Gabler, J.W. Ross, Functions of manganese in reproduction, *Animal Reproduction Science*, **2022**, *238*, 106924. [[Crossref](#)], [[Google Scholar](#)], [[Publisher](#)]
- [22] T.J. Wang, K. Liu, X. Shi, L. Ye, W. Gu, C.X. Yan, Tuning of synthesis conditions by thermal decomposition towards gadolinium-doped manganese carbonate nanoparticles with uniform size and high relaxivity, *New Journal of Chemistry*, **2017**, *41*, 225-230. [[Crossref](#)], [[Google Scholar](#)], [[Publisher](#)]
- [23] S.H. Lee, Y. Kwon, S. Park, M. Cho, Y. Lee, Facile synthesis of MnCO<sub>3</sub> nanoparticles by supercritical CO<sub>2</sub> and their conversion to manganese oxide for supercapacitor electrode materials, *Journal of Materials Science*, **2015**, *50*, 5952-5959. [[Crossref](#)], [[Google Scholar](#)], [[Publisher](#)]
- [24] Y. Lu, R. Gao, J. Song, W. Li, G. Hu, Synthesis of manganese carbonate templates with different morphologies and their application in preparing hollow MoS<sub>2</sub> micro/nanostructures for photocatalysis, *Journal of Nanoscience and Nanotechnology*, **2020**, *20*, 2239-2246. [[Crossref](#)], [[Google Scholar](#)], [[Publisher](#)]
- [25] M. Mavioglu Kaya, H.A. Deveci, I. Kaya, N. Atar, M.L. Yola, The electrochemical detection of ochratoxin a in apple juice via mnco<sub>3</sub> nanostructures incorporated into carbon fibers containing a molecularly imprinting polymer, *Biosensors*, **2023**, *13*, 760. [[Crossref](#)], [[Google Scholar](#)], [[Publisher](#)]
- [26] J. Fei, S. Zhao, X. Bo, F. Xie, G. Li, E.A.M. Ahmed, Q. Zhang, H. Jin, Z. Lin, Nano- single-crystal- constructed submicron MnCO<sub>3</sub> hollow spindles enabled by solid precursor transition combined Ostwald ripening in situ on graphene toward exceptional interfacial and capacitive lithium storage, *Carbon Energy*, **2023**, *5*, 333. [[Crossref](#)], [[Google Scholar](#)], [[Publisher](#)]
- [27] Y. Jiang, X. Liao, W. Tang, C. Huang, Y. Pan, S. Ning, Platelet membrane biomimetic manganese carbonate nanoparticles promote breast cancer stem cell clearance for sensitized radiotherapy, *International Journal of Nanomedicine*, **2024**, 1699-1707. [[Crossref](#)], [[Google Scholar](#)], [[Publisher](#)]
- [28] S. Meng, D. Qin, Y. Wu, G. Mo, X. Jiang, B. Deng, Electrochemiluminescence resonance energy transfer of MnCO<sub>3</sub> for ultrasensitive amyloid- $\beta$  protein detection, *Talanta*, **2023**, *253*, 123993. [[Crossref](#)], [[Google Scholar](#)], [[Publisher](#)]
- [29] C.C. Coelho, T. Padrão, L. Costa, M.T. Pinto, P.C. Costa, V.F. Domingues, P.A. Quadros, F.J. Monteiro, S.R. Sousa, The antibacterial and angiogenic effect of magnesium oxide in a hydroxyapatite bone substitute, *Scientific Reports*, **2020**, *10*, 19098. [[Crossref](#)], [[Google Scholar](#)], [[Publisher](#)]
- [30] S.S. Shendage, K. Gaikwad, K. Kachare, S. Kashte, A.V. Ghule, In vitro and in vivo study of copper-doped bioactive glass for bone regeneration application, *Materials Chemistry and Physics*, **2024**, *313*, 128789. [[Crossref](#)], [[Google Scholar](#)], [[Publisher](#)]
- [31] I. Rzhepakovsky, S. Piskov, S. Avanesyan, M. Sizonenko, L. Timchenko, O. Anfinogenova, A. Nagdalian, A. Blinov, E. Denisova, S. Kochergin, S. Kubanov, Composite of bacterial cellulose and gelatin: A versatile biocompatible scaffold for tissue engineering, *International Journal of Biological*

- Macromolecules*, **2024**, 256, 128369. [Crossref], [Google Scholar], [Publisher]
- [32] W. Underwood, R. Anthony, AVMA guidelines for the euthanasia of animals: 2020 edition, Retrieved on March, **2020**, 2013, 2020-1. [Google Scholar], [Publisher]
- [33] B. Ali, M.R. Shakir, M.A. Iqbal, Techniques in the synthesis of mononuclear manganese complexes: A review, *Reviews in Inorganic Chemistry*, **2017**, 37, 105-130. [Crossref], [Google Scholar], [Publisher]
- [34] N. Samadani Langeroodi, Z. Farhadraresh, A. Dehno Khalaji, Optimization of adsorption parameters for Fe (III) ions removal from aqueous solutions by transition metal oxide nanocomposite, *Green Chemistry Letters and Reviews*, **2018**, 11, 404-413. [Crossref], [Google Scholar], [Publisher]
- [35] A. Anžlovar, M. Marinšek, Z.C. Orel, M. Žigon, Basic zinc carbonate as a precursor in the solvothermal synthesis of nano-zinc oxide, *Materials & Design*, **2015**, 86, 347-353. [Crossref], [Google Scholar], [Publisher]
- [36] W. Liang, J. Bai, Z. Li, Y. Meng, K. Liu, L. Li, Crystal growth, structure and thermal properties of anhydrous zinc carbonate ( $ZnCO_3$ ), *Journal of Alloys and Compounds*, **2022**, 898, 162916. [Crossref], [Google Scholar], [Publisher]
- [37] S. Anandan, B.G.S. Raj, G.J. Lee, J.J. Wu, Sonochemical synthesis of manganese (II) hydroxide for supercapacitor applications, *Materials Research Bulletin*, **2013**, 48, 3357-3361. [Crossref], [Google Scholar], [Publisher]
- [38] D. Wei, J. Liu, Z. Luo, X. Xie, Insight into the reactions of antimonite with manganese oxides: Synergistic effects of Mn (III) and oxygen vacancies, *Water Research*, **2023**, 232, 119681. [Crossref], [Google Scholar], [Publisher]
- [39] N.A. Nik Aziz, N.K. Idris, M.I.N. Isa, Solid polymer electrolytes based on methylcellulose: FT-IR and ionic conductivity studies, *International Journal of Polymer Analysis and Characterization*, **2010**, 15, 319-327. [Crossref], [Google Scholar], [Publisher]
- [40] M.S. Ali, P. Bhunia, A.P. Samanta, J.T. Orasugh, D. Chattopadhyay, Transdermal therapeutic system: Study of cellulose nanocrystals influenced methylcellulose-chitosan bionanocomposites, *International Journal of Biological Macromolecules*, **2022**, 218, 556-567. [Crossref], [Google Scholar], [Publisher]
- [41] E.S. Abdel-Halim, Chemical modification of cellulose extracted from sugarcane bagasse: Preparation of hydroxyethyl cellulose, *Arabian Journal of Chemistry*, **2014**, 7, 362-371. [Crossref], [Google Scholar], [Publisher]
- [42] G.F. El Fawal, M.M. Abu-Serie, M.A. Hassan, M.S. Elnouby, Hydroxyethyl cellulose hydrogel for wound dressing: Fabrication, characterization and in vitro evaluation, *International Journal of Biological Macromolecules*, **2018**, 111, 649-659. [Crossref], [Google Scholar], [Publisher]
- [43] C.R. Buhr, N. Wiesmann, R.C. Tanner, J. Brieger, J. Eckrich, The chorioallantoic membrane assay in nanotoxicological research—An alternative for in vivo experimentation, *Nanomaterials*, **2020**, 10, 2328. [Crossref], [Google Scholar], [Publisher]
- [44] S. Vimalraj, S. Renugaa, A. Dhanasekaran, Chick embryo chorioallantoic membrane: a biomaterial testing platform for tissue engineering applications, *Process Biochemistry*, **2023**, 124, 81-91. [Crossref], [Google Scholar], [Publisher]
- [45] N. Kohli, P. Sawadkar, S. Ho, V. Sharma, M. Snow, S. Powell, M.A. Woodruff, L. Hook, E. García-Gareta, Pre-screening the intrinsic angiogenic capacity of biomaterials in an optimised ex ovo chorioallantoic membrane model, *Journal of Tissue Engineering*, **2020**, 11, 2041731420901621. [Crossref], [Google Scholar], [Publisher]
- [46] D. Ribatti, The chick embryo chorioallantoic membrane (CAM), A

multifaceted experimental model, *Mechanisms of Development*, **2016**, *141*, 70-77. [[Crossref](#)], [[Google Scholar](#)], [[Publisher](#)]

[47] T.I. Valdes, D. Kreutzer, F. Moussy, The chick chorioallantoic membrane as a novel in vivo model for the testing of biomaterials, *Journal of Biomedical Materials Research: An Official Journal of The Society for Biomaterials, The Japanese Society for Biomaterials, and The Australian Society for Biomaterials and the Korean Society for Biomaterials*, **2002**, *62*, 273-282. [[Crossref](#)], [[Google Scholar](#)], [[Publisher](#)]

**How to cite this article:** Andrey Blinov, Zafar Rekhman, Alexey Gvozdenko, Sergey Piskov, Vadim Agzamov, Nikita Omelianov, Zelimhan Chagaev, Daria Morzaleva, Iuliia Ismagilova, Daria Gadaeva, Marina Poladashvili, Andrey Nagdalian, Synthesis, characterization and biocompatibility assessment of manganese carbonate nanoparticles stabilized with methylcellulose for multifaceted application in medicine. *Journal of Medicinal and Pharmaceutical Chemistry Research*, 2024, 7(9), 1821-1837. **Link:** [https://jmpcr.samipubco.com/article\\_211320.html](https://jmpcr.samipubco.com/article_211320.html)